

A floating 3D silicon microprobe array for neural drug delivery compatible with electrical recording

S Spieth^{1,5}, O Brett², K Seidl³, A A A Aarts⁴, M A Erismis⁴, S Herwik³,
F Trenkle², S Tätzner¹, J Auber¹, M Daub², H P Neves⁴, R Puers⁴,
O Paul³, P Ruther³ and R Zengerle^{1,2}

¹ Institut für Mikro- und Informationstechnik der Hahn-Schickard-Gesellschaft e.V. (HSG-IMIT), Villingen-Schwenningen, Germany

² Laboratory for MEMS Applications, Department of Microsystems Engineering (IMTEK), University of Freiburg, Freiburg, Germany

³ Microsystem Materials Laboratory, Department of Microsystems Engineering (IMTEK), University of Freiburg, Freiburg, Germany

⁴ Interuniversity Microelectronics Center (IMEC), Leuven, Belgium

E-mail: sven.spieth@hsg-imit.de

Received 14 June 2011, in final form 17 September 2011

Published 3 November 2011

Online at stacks.iop.org/JMM/21/125001

Abstract

This paper reports on the design, fabrication, assembly and characterization of a three-dimensional silicon-based floating microprobe array for localized drug delivery to be applied in neuroscience research. The microprobe array is composed of a silicon platform into which up to four silicon probe combs with needle-like probe shafts can be inserted. Two dedicated positions in the array allow the integration of combs for drug delivery. The implemented comb variants feature 8 mm long probe shafts with two individually addressable microchannels incorporated in a single shaft or distributed to two shafts. Liquid supply to the array is realized by a highly flexible 250 μm thick multi-lumen microfluidic cable made from polydimethylsiloxane (PDMS). The specific design concept of the slim-base platform enables floating implantation of the array in the small space between brain and skull. In turn, the flexible cable mechanically decouples the array from any microfluidic interface rigidly fixed to the skull. After assembly of the array, full functionality is demonstrated and characterized at infusion rates from 1 to 5 $\mu\text{L min}^{-1}$. Further, the effect of a parylene-C coating on the water vapour and osmotic liquid water transport through the PDMS cable walls is experimentally evaluated by determining the respective transmission rates including the water vapour permeability of the used PDMS type.

(Some figures in this article are in colour only in the electronic version)

1. Introduction

One of the primary goals of neuroscience is the basic understanding of electrophysiological processes in the brain which are the basis for sensory perception, thinking, decision making and motor function and may hold the key for the treatment of brain-related diseases. Since information is

transmitted among the building blocks of the brain, i.e. the neurons, by electrical as well as chemical signals [1], monitoring and influencing these signal pathways is of great interest. For this purpose, a multitude of different types of microprobes which are directly inserted into the brain tissue have been developed in the past. Dependent on the number and geometrical arrangement of the probe shafts, one-dimensional (1D) single-shaft probes, two-dimensional (2D) probe combs with multiple shafts and fully three-dimensional

⁵ Author to whom any correspondence should be addressed.

(3D) microprobe arrays can be distinguished. Additionally, acute and chronic probes have to be differentiated. Whereas acute probes are only operated during a neurological surgery and are typically fixed to laboratory equipment, chronic probes are implanted over a longer period of time.

Wire electrodes for recording and stimulation of electrical signals [2] as well as glass or steel capillaries used to deliver pharmaceutical substances directly into the brain [3] are the established tools in neuroscience research. However, the rapid development of microelectromechanical systems (MEMS) within the last decades has opened completely new technological perspectives with respect to system integration [4]. In particular, the applied microfabrication processes based on deep reactive ion etching (DRIE) enable a high degree of freedom in probe design combined with the possibility of integrating multiple functionalities, as detailed in the following.

To investigate the organization of neurons and to cover larger areas of the brain, 3D arrays are required. However, particularly chronically implanted 3D microprobe arrays demand high standards of the entire array concept. As an example, blood pulsation and head movements cause permanent relative motions of the brain with respect to the surrounding skull. Since the array has to be implanted in the small space between skull and brain, it is subjected to all of these relative movements. Therefore, the array must be mechanically decoupled from the skull and be able to float on the cerebral cortex in order to minimize tissue damage. To realize this, the backbone of the array should be made as thin as possible and all connecting elements, e.g. electrical as well as fluidic cables, must be highly elastic to minimize any mechanical interference with the floating operation of the array.

Various floating 3D arrays based on wire electrodes have been proposed, some of them being already commercially available [5, 6]. They are fabricated by assembling individual wire electrodes into a common platform made from ceramics [7] or epoxy [8]. However, these arrays are limited in functionality as the number of recording sites equals that of the assembled wires. Additional functionalities such as fluidic delivery have not been addressed yet.

On the other hand, silicon-based floating 3D probe arrays realized using MEMS fabrication processes have attracted growing attention over the past decades. Restricted by the general concept of micromachining thin silicon wafers and the subtractive nature of the available shaping processes, two fabrication technologies can be distinguished: in- and out-of-plane fabrication sequences.

In the case of out-of-plane fabrication, microprobe shafts oriented perpendicularly to the wafer plane are fabricated by removing excess bulk material. Consequently, the length of the probe shafts cannot exceed the wafer thickness. Among the out-of-plane probe arrays, the so-called Utah array [9], commercialized by Blackrock Microsystems, Salt Lake City, UT, USA, is certainly the most popular structure. Although the array is considered to be robust and allows the hybrid integration of CMOS electronics on the rear of the backbone [10], the probe shafts are currently restricted to a length of

1.5 mm comprising one tip electrode per shaft only. An additional fluidic functionality has not been presented so far. Nonetheless, the incorporation of fluidic microchannels into out-of-plane probes has been extensively investigated in the field of transdermal drug delivery [11]. However, the rather short probes of a few hundred micrometers in length are not practical for neural applications where probe lengths on the order of millimetres are required.

Alternatively, 1D probes and 2D probe combs can be fabricated in the wafer plane using in-plane fabrication technologies. This enables shafts with lengths of several millimetres combined with multiple electrodes for electrical recording [12–14] or stimulation [15, 16] as well as monolithic integration of electronic circuits [17, 18], fluidic microchannels [19, 20] and biosensors [21, 22] to be realized. Following the pioneering work of Wise *et al* [23], a wide variety of such probes have been developed in the past decades. Particularly well known are the so-called Michigan probes which are commercially available through NeuroNexus Technologies Inc., Ann Arbor, MI, USA.

Different approaches have been presented to accomplish the transition from 2D combs to 3D arrays based on through-hole assembly [12, 24–26] or insertion [27–29] of probe combs into a common platform, direct stacking of probe combs [30–32] as well as folding [33] of flexible polyimide substrates including self-assembly approaches [34]. However, up to now only selected approaches are feasible to realize the thin backbone required for a floating operation of the array. Furthermore, although the feasibility of multifunctional probes has been demonstrated in 2D, no microprobe arrays that include functionalities beyond electrical recording combined with CMOS circuitry are currently available. In particular, the incorporation of the liquid handling capability into a floating microprobe array opens completely new perspectives with respect to drug delivery, microdialysis and *in situ* calibration of biosensors. Furthermore, the combination of recording electrodes with drug delivery allows both electrical and chemical processes to be influenced in the brain.

One reason for the lack of floating arrays with drug delivery capability is the increased complexity of liquid handling in comparison to the electrical access to neural signals. Liquid delivery relies on the physical transport of a liquid, which necessitates not only conductive connections but also fluidic microchannels and connections [35]. Consequently, suitable fabrication and assembly technologies are required for the incorporation of fluidic microchannels into a 3D array. Moreover, in order to realize liquid supply and enable floating operation, a highly flexible multi-lumen microfluidic cable comparable in its mechanical properties to the polyimide [36, 37] or parylene [30, 38] ribbon cables used for electrical connection of floating arrays is requested.

Thin and flexible microfluidic structures have previously been fabricated by lamination of polyimide layers [39] or deposition of parylene applying either sacrificial photoresist [40] or bonding techniques [41]. However, both materials cannot bond without further means to silicon or silicon oxide. This complicates their assembly with standard

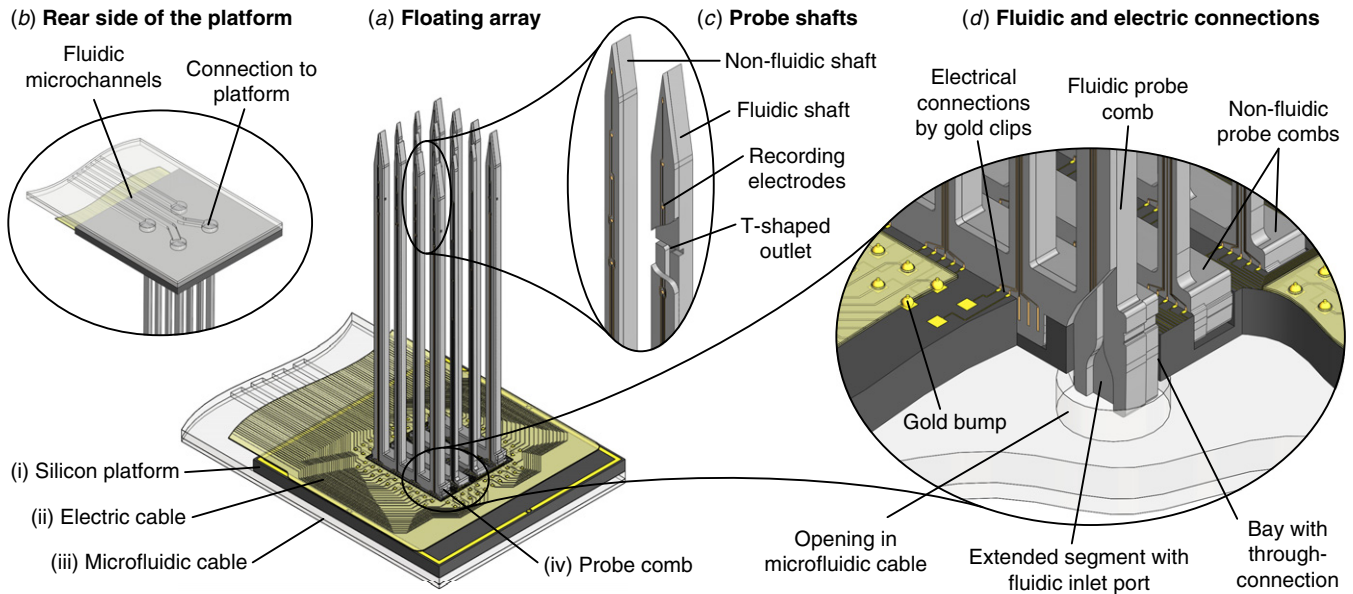


Figure 1. (a) Illustration of a floating 3D array for electrode recording and drug delivery. Additional views show (b) the rear side of the platform with the microfluidic cable for liquid supply, (c) non-fluidic as well as fluidic probe shafts, and (d) a sectional view showing the envisaged fluidic and electric connections.

MEMS materials. On the other hand, silicone rubbers or polydimethylsiloxanes (PDMS) are highly elastic and can bond after oxygen plasma activation directly to a broad variety of materials including silicon and silicon oxide [42]. Moreover, PDMS can be precisely patterned by soft lithography [43]. As far as the chronic application of silicones in humans is concerned, use of these materials as part of implants has been documented at least since 1947 [44]. Furthermore, PDMS-based electrode arrays have previously been realized for neural applications [45, 46], and the material was additionally suggested for flexible interconnects [47]. For these reasons, PDMS is seen as a favourite material candidate for the fabrication of microfluidic cables in conjunction with implantable silicon 3D arrays.

The work presented in this paper has been performed within the EU-funded *NeuroProbes* project [48, 49] aiming at the development of multifunctional 1D, 2D and 3D neural probe arrays. This paper presents the first floating 3D microprobe array for neural drug delivery which allows liquids to be infused through individual probe shafts and is fully compatible with the integration of recording electrodes [37, 50], CMOS electronics [14, 18, 51] and sensing elements such as amperometric biosensors [22] for the detection of neurotransmitters. The selected fluidic system concept including two different assembly strategies is detailed in section 2. Thereby, the electric requirements of a future multifunctional floating 3D array are also considered. The layout and fabrication of the different system components as well as the assembly of the complete array are described in section 3. Finally, the fluidic properties of an assembled array and the effect of a parylene-C coating on the diffusive water vapour and osmotic liquid water transport through the microfluidic cable walls is experimentally evaluated in section 4.

2. System design

The microfluidic integration concept presented in this study is compatible to the 3D electrode arrays for cerebral applications [27, 50] developed within the EU-project *NeuroProbes* [48, 49]. It addresses the fluidic requirements of the ultimate goal of a multifunctional floating 3D array for electrical recordings combined with localized drug delivery. As illustrated in figure 1(a), such an array comprises (i) a slim-base silicon platform, separate cables for (ii) electrical interconnection as well as (iii) microfluidic liquid supply, and (iv) probe combs with slender probe shafts containing electrodes and fluidic microchannels. The system layout used in this study applies a slim-base platform offering 4×4 bays for the integration of four probe combs. However, the design space is not limited to this specific number of combs.

The electrical interconnection scheme of the platform is based on gold clips protruding over the edge of the platform bays and corresponding rectangular contact pads integrated on extended probe comb segments (cf figure 1(d)). As described in detail elsewhere [50], the electrical contact between the platform clips and the comb pads is achieved upon insertion of the comb segments into the platform bays. Thereby, the gold clips are bent down and squeezed between the comb segments and bay sidewalls resulting in the electrical contact between both components. Platform layouts comprising five or eleven clips per bay have been presented so far [50, 51].

The gold clips are connected via metal leads to bond pads arranged along the perimeter of the platform. The electrical interconnection of these platform bond pads to the external recording instrumentation is realized using highly flexible polyimide (PI) ribbon cables [37, 52]. The cable assembly applies the MicroFlex technology [53] in combination with a polymeric underfill and a silicone-based encapsulation [27].

Alternatively, a cable assembly technology based on flip-chip-bonding might be applied as well [54].

As the integration of the fluidic functionality must not interfere with the electrical platform components, the liquid supply of the probes is realized from the platform rear (cf figure 1(d)) using a flexible PDMS cable with integrated microfluidic channels (cf figure 1(b)). In the platform itself, the two outer probe combs comprise two fluidic microchannels. To access these microchannels, the four platform bays in the corners of the 4×4 array are implemented as through-connections to the platform rear as shown in the sectional view in figure 1(d). In any case, the fluidic bays may include gold clips for the electrical interconnection of the probes as well.

The probe combs comprise a wider probe base to connect the individual probe shafts and base segments to be inserted into the platform bays. As shown in figure 1(d), non-fluidic as well as fluidic probe combs have been realized. The non-fluidic probe combs comprise four shorter base segments carrying rectangular contact pads. In contrast, the two outer segments of the fluidic probe combs are elongated and comprise an additional in-plane inlet port for the liquid supply of a probe shaft. These fluidic base segments protrude from the platform rear such that the inlet ports fit into the respective openings in the microfluidic cable, as indicated in the sectional view in figure 1(d).

Two scenarios can be distinguished in view of the assembly strategy of the entire 3D array, as illustrated in figure 2. Major differences are related to the leakage-free sealing of the fluidic probe segments in the platform, i.e. whether the sealing is applied from the platform rear or from the bay side. This affects the order in which the probe combs and the microfluidic cable have to be assembled to the platform. Independently of the assembly strategy, the electrical polyimide ribbon cable has to be first bonded to the bay side of the platform (cf figure 2(b)).

In case the sealing of the fluidic inlet segments is performed from the platform rear, the probe combs are first inserted into the platform and sealed with an adhesive applied from the rear (cf figure 2(c1)). This is followed by the bonding of the microfluidic cable, as illustrated in figure 2(d1). As the platform rear comprises only the four through openings, dedicated channel structures may be incorporated which are used to guide and localize the adhesive during the sealing process.

This sealing approach has been verified using simplified test platforms and test probes realized using DRIE, as illustrated in figure 3. These test platforms incorporate two bays of $400 \times 303 \mu\text{m}^2$, one of which is implemented as a through-connection. The corresponding probe bases with a thickness of $300 \mu\text{m}$ comprise two segments of different lengths fitting exactly into these bays. Upon test probe insertion, the longer segment protrudes by $100 \mu\text{m}$ over the platform rear. The segment is surrounded by a channel structure in the platform rear connected to a larger dispensing area used to apply the adhesive (cf figure 3(a)). Figure 3(b) shows a sequence of optical micrographs illustrating the distribution of the adhesive (EPO-TEK[®] 353ND, Polytec PT GmbH, Waldbronn, Germany) by capillary forces in the

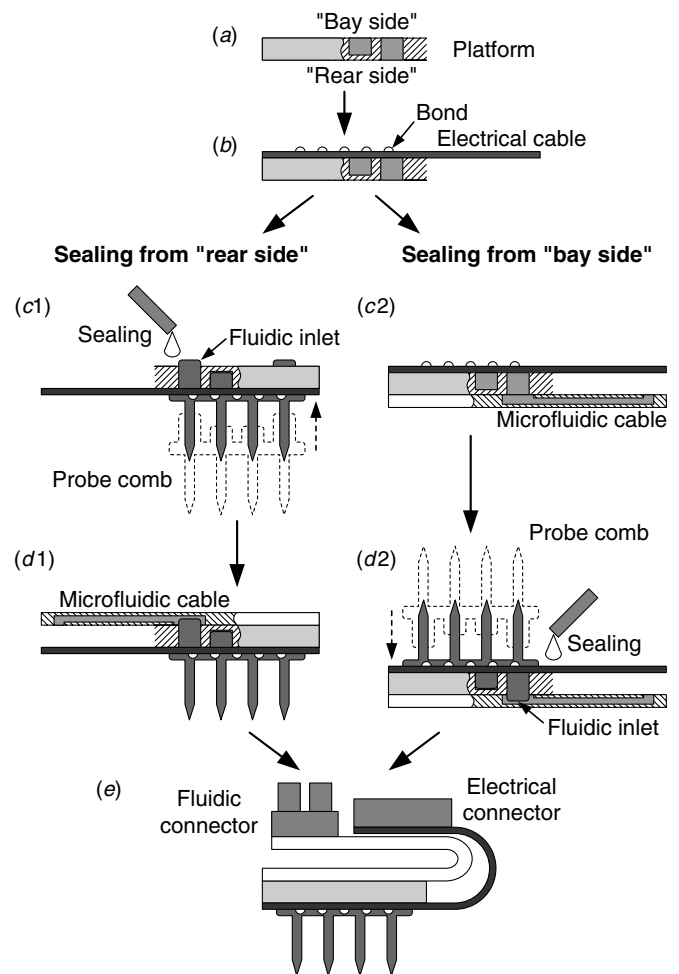


Figure 2. Two alternative assembly sequences of the electro-fluidic microprobe array differing in the sealing of the fluidic combs from the rear and bay sides of the platform: (a), (b) assembly of the electric cable to the platform, (c1) insertion of the probe combs and sealing from the rear side followed by (d1) bonding of the microfluidic cable; alternatively, (c2) bonding of the microfluidic cable on the rear side followed by (d2) insertion and sealing of the probe combs from the bay side, and (e) assembly of the fluidic and electrical connectors.

narrowing channel structure around the probe segment. As the segment protrudes above the platform surface, the adhesive cannot reach that part of the segment which in the case of the fluidic probes comprises the liquid inlet port. This approach prevents the blockage of the integrated fluidic microchannels of the probe. Based on these test structures, it can be concluded that this sealing process is very robust and elegant.

Alternatively, the microfluidic cable can be first bonded to the rear side of the platform followed by the insertion and sealing of the combs from the bay side, as shown in figures 2(c2), (d2). This is of particular interest since sealing of the fluidic probe combs is achieved in the same processing step performed to fill the remaining gaps between probe segments and the bay sidewalls as well as the encapsulation of the stud bumps used for the assembly of the electrical cable [27]. The gaps around the protruding comb segments will effectively serve as a capillary stop to prevent any adhesive from entering the fluidic microchannels in the cable. Therefore, this concept

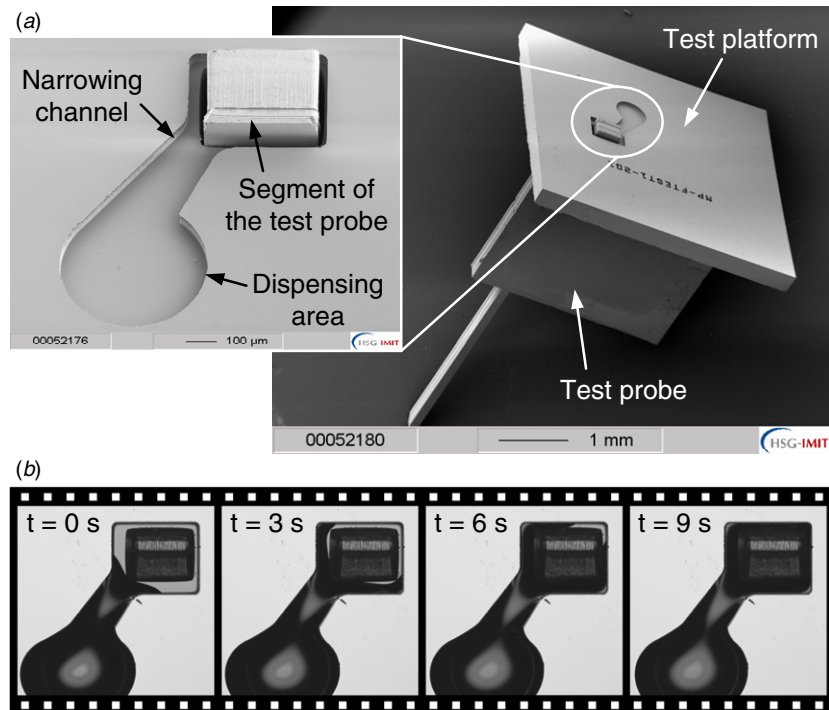


Figure 3. Test platform and probe for verification of the sealing approach from the platform rear side; (a) dispensing area and associated narrowing channel to guide the adhesive around the protruding segment of the probe comb, (b) optical micrograph sequence showing how the adhesive is guided in the channel structure by capillary forces.

was verified using bare test platforms having no channel structures for adhesive dispensing.

The last assembly step is again identical for both strategies and does not directly involve the silicon platform anymore. This step includes the attachment of the electric and fluidic connectors to the polyimide ribbon and microfluidic cable, respectively.

Both assembly strategies are compared in table 1. While the rear-side sealing utilizes a more complex platform design requiring additional processing steps, the application of the adhesive is well controlled due to the implemented dispensing area and guiding structure. However, the area available for bonding of the microfluidic cable is reduced. Moreover, the consecutive assembly steps have to be performed using a platform with already inserted probe combs. This requires specific care to avoid any probe shaft fracture. In the case of the bay-side sealing, the conventional platform design which provides the largest bonding area for the microfluidic cable can be applied. On the other hand, the adhesive has to be dispensed close to the fragile probe shafts. Taking all arguments into account, it can be concluded that the bay-side sealing is more attractive especially because of the less critical handling of the array.

Previously, the assembly of full 3D electrode arrays has been demonstrated and the functionality was successfully verified by *in vivo* recordings [27]. Having achieved this important milestone, this paper concentrates now on the microfluidic integration concept for such an array being the key aspect in view of liquid drug delivery for stimulation and inactivation of neural tissue.

3. Layout and fabrication

The floating fluidic array presented in this publication corresponds to the schematic shown in figure 1 except for the electric components. An exploded view of the implemented floating array with the corresponding component layouts is shown in figure 4. The complete array is composed of a microfluidic adapter, a multi-lumen microfluidic PDMS cable, a silicon platform and two silicon probe comb variants. In the following subsections, first the fabrication technologies of the different components are described. This is followed by a description of the assembly according to the sequence for probe sealing from the bay side, as illustrated on the right-hand side of figure 2.

3.1. Fluidic microprobe combs

Two fluidic comb types, termed P1 and P2, have been designed. They are shown in figure 4(d). The geometrical dimensions of the probe base and segments for mechanical, fluidical and future electrical interconnection are identical in both cases. The probe base has a thickness of $300 \mu\text{m}$ and is $2020 \times 325 \mu\text{m}^2$ in size. It comprises two segments of $390 \times 220 \mu\text{m}^2$ in the centre and two segments of $390 \times 420 \mu\text{m}^2$ towards the edges of the base used as fluidic inlet ports. As the segments in the centre are $25 \mu\text{m}$ longer than the respective depth of the platform bays, a gap remains between the comb base and the platform surface promoting the adhesive distribution during sealing. The probe type P1 comprises four probe shafts in total. The two outer shafts incorporate one fluidic microchannel each and are aligned with the fluidic inlet ports. The two shafts in the

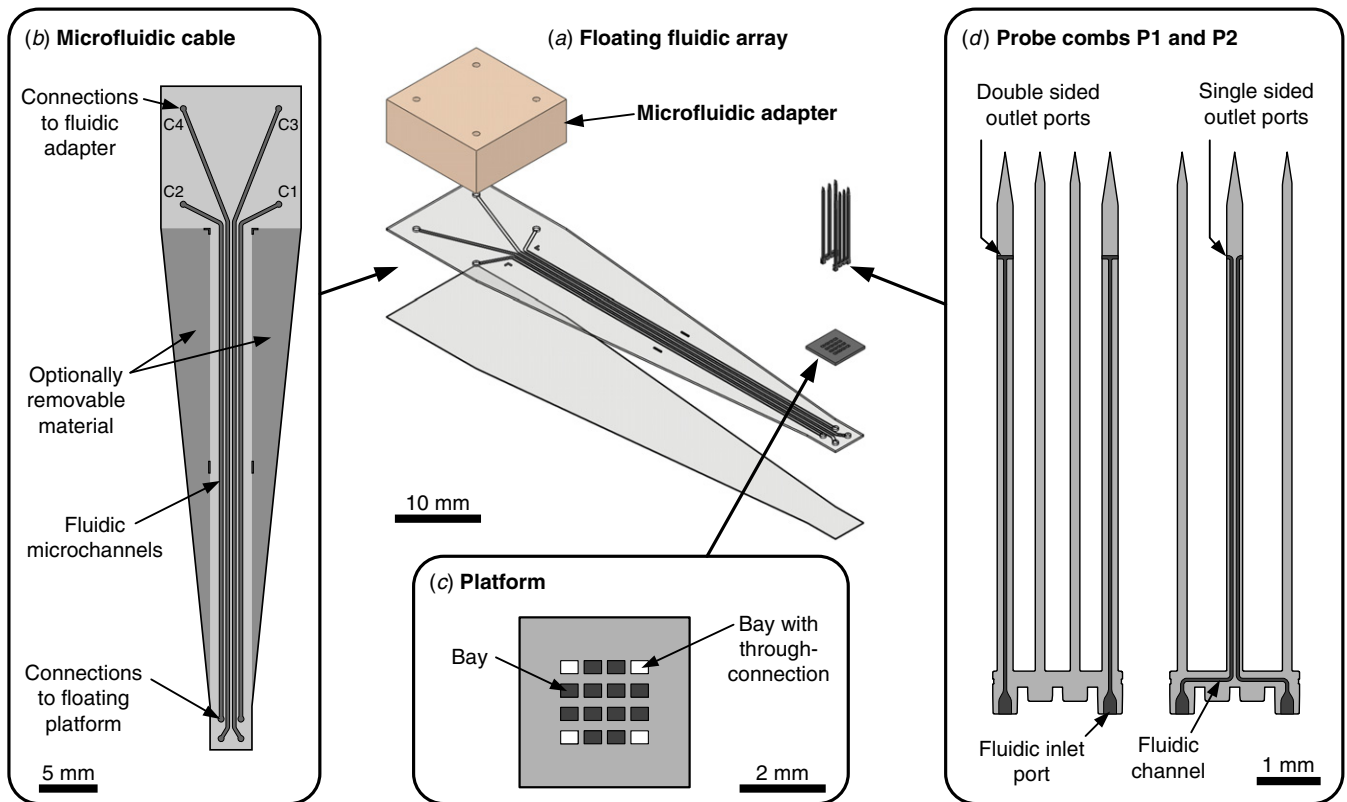


Figure 4. (a) Exploded view of the floating fluidic array and layouts of the different components; besides the microfluidic adapter this includes (b) a multi-lumen microfluidic cable, (c) a silicon platform and (d) two different probe comb variants with one or two fluidic microchannels integrated in one shaft.

Table 1. Comparison of the sealing methods: ‘rear side’ and ‘bay side’.

Sealing from rear side	Sealing from bay side
<ul style="list-style-type: none"> + Microchannels to guide adhesive + No blockages of inlet ports by adhesive + No space constraints due to probe shafts 	<ul style="list-style-type: none"> + No process steps for adhesive channels + Maximized bonding area for microfluidic cable + No fixation of probe combs standing upright + Only one assembly step with inserted combs
<ul style="list-style-type: none"> – Additional processing steps for adhesive microchannels – Reduced bonding area for microfluidic cable – Fixation of probe combs flipped upside down – Two assembly steps with inserted combs 	<ul style="list-style-type: none"> – No precise localization of adhesive on bay side – Space constraints due to probe shafts – Increased risk of adhesive entering the cable

middle are designed to carry electrodes in a future version of the 3D array. Although the position of the liquid inlet ports is given by the location of the comb segments, the probe base can be used for liquid distribution as it is the case for the probe type P2. This probe has one central shaft with two microchannels and two surrounding shafts designed for electrode integration. In this case, the probe base is used to join the microfluidic channels into one probe shaft. Using this approach, the shafts with microchannels can be placed at virtually any position on the probe base.

The shafts comprising microchannels have a rectangular cross-sectional area of $250 \times 200 \mu\text{m}^2$, whereas the shafts reserved exclusively for electrodes are narrowed down to $150 \times 200 \mu\text{m}^2$. The length of all shafts is $8150 \mu\text{m}$. The rectangular cross-section of the microchannels narrows rapidly from $200 \times 50 \mu\text{m}^2$ at the inlet ports to $50 \times 50 \mu\text{m}^2$ along the probe shafts.

The outlet ports of the fluidic channels are implemented in the shaft flanks. The probe type P1 has a T-shaped outlet with openings on both flanks of the shaft. Previous experiments demonstrated that this outlet configuration reduces liquid backflow along the shaft and promotes localized liquid dispensing [55]. Since the probe type P2 has two separate microchannels incorporated in one shaft, the respective outlets are located on the opposite sides of the shaft. However, it is also possible to implement both outlets at different positions on one side of the shaft.

The fabrication process of the fluidic probe combs is a modification of the two-wafer bond process developed in the framework of the *NeuroProbes* project [20]. The five-mask fabrication process is summarized in figure 5. It starts with the dry etching of 150 nm deep alignment marks on the rear of 250 μm thick, double-side-polished, 4" (100)-wafers. These marks ensure the precise alignment of all

subsequent photolithography masks. This is followed by the thermal oxidation of the wafers providing a 300 nm thick protective layer on the wafer rear during the following dry etching steps. An additional 2 μm thick silicon oxide (SiO_x) layer is deposited on the front side of the channel wafer using plasma enhanced chemical vapour deposition (PECVD). This oxide layer is patterned by reactive ion etching (RIE), as schematically shown in figure 5(a). The used mask layout comprises the channel structure as well as the shape of the probe combs, i.e. shafts and probe base. The SiO_x layer serves as the masking layer in the subsequent two-stage DRIE process performed in an inductively coupled plasma (ICP) etcher (ICP Cluster, STS, Newport, UK). In order to define the channel depth independently of the depth of the trenches delimiting the outer probe geometry, the mask openings for the fluidic channels are first covered by a photolithographically structured 5 μm thick photoresist (AZ4533, MicroChemicals GmbH, Germany) which serves as an additional soft mask as shown in figure 5(b). The outer probe shape is then etched in a first DRIE step to a depth of 100 μm . After the removal of the AZ4533 photoresist, the fluidic channels are defined in a second DRIE step to a depth of 50 μm (figure 5(c)). Consequently, the probe shape is further etched to a total depth of 150 μm , as indicated in figure 5(c).

Next, the thermal and PECVD silicon oxides are removed by wet etching. This is followed by thermal oxidation of the channel as well as cover wafers to an oxide thickness of 500 nm required for the subsequent wafer-to-wafer bonding steps. Aside from their need for the wafer bonding process, the silicon oxide layers serve as an etch stop. They prevent a non-uniform opening of the buried cavities within the wafer bond during the last two DRIE steps (cf figures 5(f), (g)) and consequently avoid uncontrolled overetching. Moreover, the fluidic channel walls become completely passivated by oxide. Thus, their biostability with respect to the applied liquids is improved.

Prior to wafer-to-wafer bonding, both wafers are RCA-cleaned to promote the formation of hydrophilic groups on the wafer surfaces. As the cover wafer is not structured before bonding, no wafer alignment is required in this case. The wafers are bonded using direct wafer bonding and annealed at 1050 $^\circ\text{C}$. During bonding, special precautions have to be taken to keep the pressure level within the channel cavities low enough to be compatible with the subsequent DRIE steps in vacuum. The bonding step is followed by the thinning of the cover wafer to a thickness of 50 μm using a commercial grinding and polishing process (Disco Hi-Tec Europe, Munich, Germany). The resulting, approximately 300 μm thick wafer stack is illustrated in figure 5(d). The achieved surface roughness of 14 nm is sufficiently low for the further processing steps.

Since the thickness of the waferstack corresponds to the thickness of the segments to be inserted into the platform bays, this dimension needs to be precisely controlled. Therefore, the thickness of the waferstack is first determined by a contactless wafer geometry gauge (MX 203, E+H Metrology, Karlsruhe, Germany) before proceeding with the processing. Based on this information, the consecutive PECVD oxides are used to

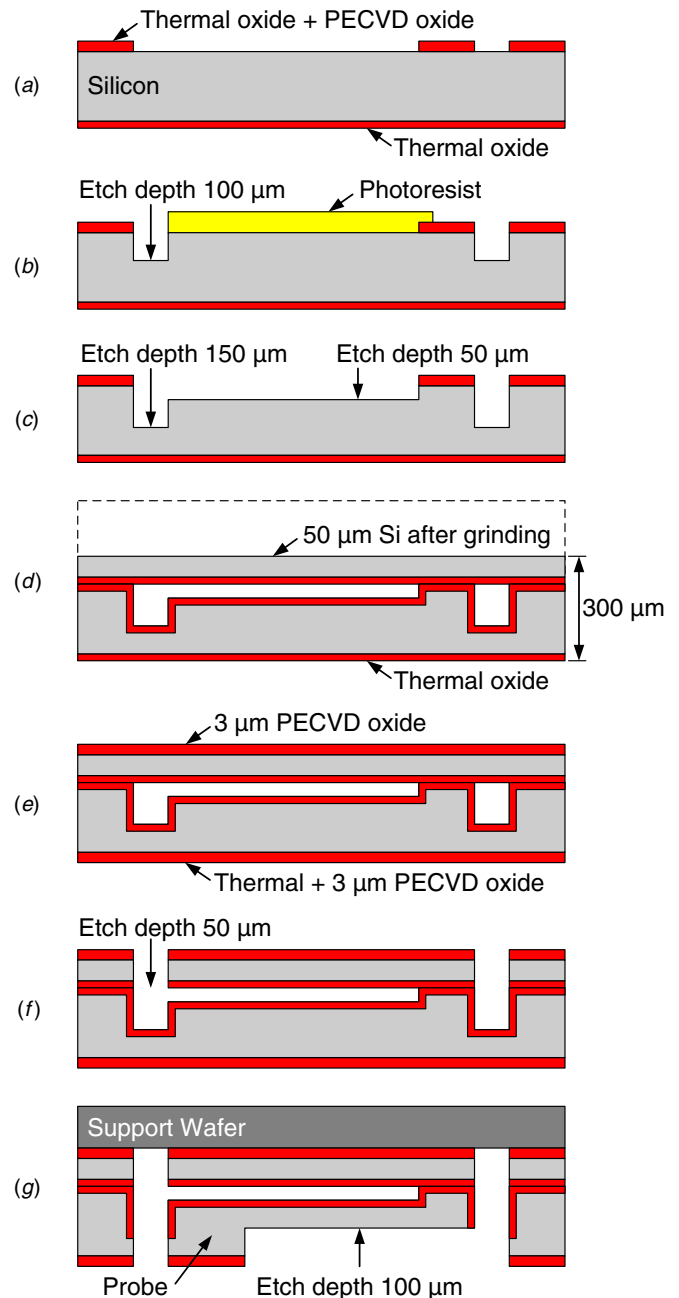


Figure 5. Fabrication process of the silicon microprobes: (a) introduction of alignment structures and deposition and patterning of the etch mask, (b), (c) two-stage DRIE process of channel structure and probe shape, (d) thermal oxidation, direct wafer-to-wafer bonding and grinding, (e) PECVD passivation layer deposition, (f), (g) rear and front side oxide patterning followed by DRIE for probe patterning, respectively.

adjust the exact thickness and to compensate for variations of the grinding process. In the present case, 3 μm PECVD oxides are deposited on both sides of the waferstack.

In the next step, a photoresist is used as a soft mask to define the overall probe shape on the front side of the waferstack. After opening the PECVD oxide by RIE, the subsequent DRIE step is performed with an etch depth equivalent to the thickness of the cover wafer. This etch step stops at the buried oxide layer of the cover wafer. The

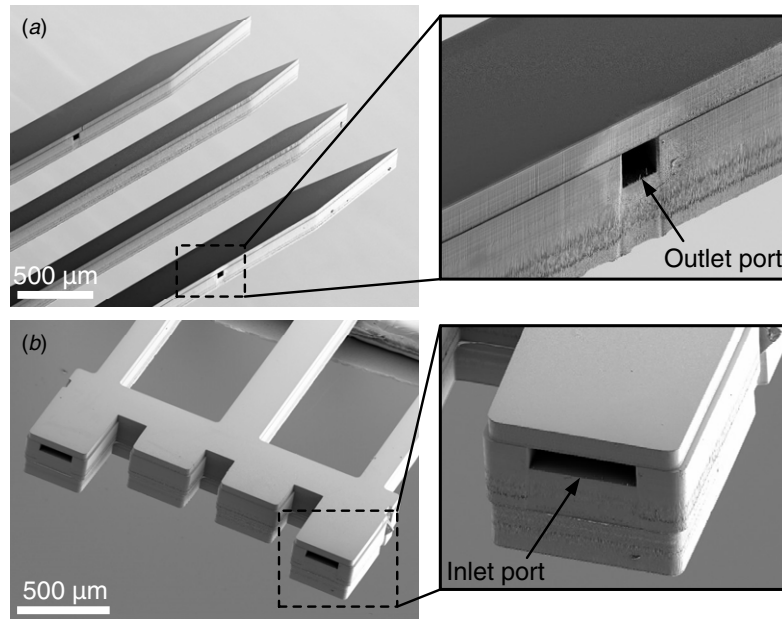


Figure 6. SEM micrographs of fabricated probe combs: (a) probe tips of a comb P1 with four shafts including fluidic outlet ports, (b) probe base of a comb P2 with three shafts having shorter segments used for mechanical stabilization and longer segments used as in-plane fluidic inlet ports.

remaining oxide membranes are subsequently removed using RIE, as illustrated in figure 5(f).

To avoid wafer fracture, the final DRIE process is performed on a support wafer. For this purpose, the front side of the wafer stack is fixed with adhesive (Crystalbond 555, SPI Supplies, West Chester, PA, USA) on a support wafer. Similarly to the patterning of the front side, the photoresist is first used as a soft mask to define the probe shape. Afterwards, the rear PECVD SiO_x as well as the thermal oxide are opened by RIE followed by a DRIE step with an etch depth of $100\ \mu\text{m}$. During this process step, the etching stops at the buried oxide of the channel wafer. In addition to the overall probe shape, this DRIE step defines the final thickness of the probe shafts. Finally, the remaining oxide membranes in the etch trenches have to be removed (cf figure 5(g)). After dissolving the adhesive to separate the wafer with probes from the support wafer, the probes are released but remain suspended in the wafer stack by thin struts [14, 20].

The scanning electron microscopy (SEM) micrographs of fabricated probe combs are shown in figure 6. Figure 6(a) shows the probe tips including liquid outlet ports for type P1, whereas figure 6(b) shows the common comb base with liquid inlet ports for type P2. The geometry and dimension of the common comb base are identical for both probe types.

3.2. Platform

The slim-base platform which serves as the backbone of the floating array has a footprint of $4000 \times 4000\ \mu\text{m}^2$ and a thickness of $300\ \mu\text{m}$. As shown in figure 4(c), it contains 4×4 bays for the assembly of up to four probe combs, as illustrated in figure 4(d). The four corner bays are implemented as through-connections to the rear side of the platform, whereas the remaining bays act as sockets only.

The platforms are realized using a two-step DRIE process combined with wafer grinding of $500\ \mu\text{m}$ thick double-side-polished, 8'' (100)-wafers, as summarized in figure 7. In a first step, the wafer is thermally oxidized to an oxide thickness of $500\ \text{nm}$. The oxide on the wafer front is then patterned by RIE using a photoresist as a soft mask to define the 4×4 bays and expose the bare silicon, as shown in figure 7(a). The SiO_2 layer serves as the masking layer in the subsequent two-stage DRIE process performed in an ICP etcher (ICP Multiplex, STS, Newport, UK).

In order to define two different etch depths of the bays, the mask openings for the bays used as sockets only are first covered by a photolithographically structured $5\ \mu\text{m}$ thick photoresist (AZ4562, MicroChemicals GmbH, Germany). The first DRIE step etches the corner bays to a depth of $110\ \mu\text{m}$, as illustrated in figure 7(b). The resist layer is then removed, exposing the remaining pattern in the oxide layer. The second DRIE step is applied by etching the newly exposed silicon to a bay depth of $195\ \mu\text{m}$, while the depth of the corner bays is increased to $305\ \mu\text{m}$ (cf figure 7(c)). The DRIE step is followed by a piranha clean which removes the polymer deposition on the sidewalls of the etched bays formed during the DRIE process. A $0.5\ \mu\text{m}$ thick PECVD silicon oxide layer is then deposited on top of the wafer and inside of the bays. Afterwards, the through-connections in the platform are realized by grinding and polishing the rear side of the wafer, as shown in figure 7(d). The resulting thickness of the platform is set to $300\ \mu\text{m}$. The polishing step is required to reduce the silicon surface roughness, improving the bonding of the microfluidic cable. Finally, the wafer is diced into individual platforms. Alternatively, the etching-before-grinding process [56] can be applied to achieve platforms of arbitrary shape including rounded corners.

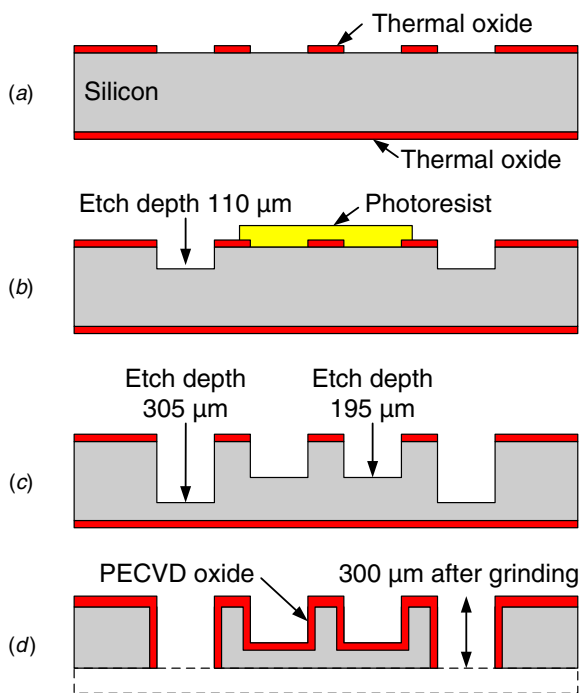


Figure 7. Fabrication process of the silicon platform: (a) deposition and patterning of the etch mask, (b), (c) two-stage DRIE of the bays, (d) deposition of the PECVD passivation layer and wafer grinding to create through-connections.

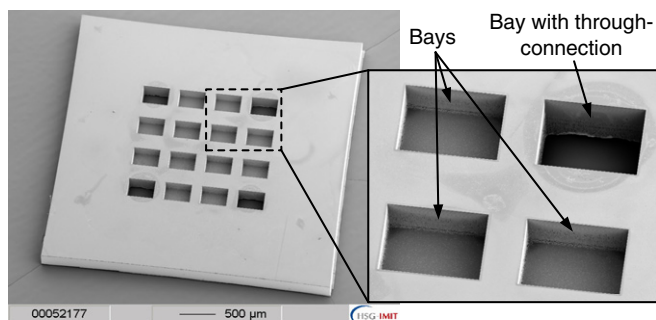


Figure 8. SEM micrograph of a fabricated silicon platform with a close-up view of the bays.

An SEM micrograph of a fabricated and diced platform is shown in figure 8. The close-up view illustrates the difference between a normal bay and a bay with through-connection.

3.3. Microfluidic cable

The layout of the multi-lumen microfluidic cable is given in figure 4(b). The flexible part of the cable between the microfluidic adapter and the floating array has a length of 40 mm and a thickness of 250 μm. The body contains four separate microfluidic channels with a width of 300 μm and a height of 50 μm. The cable connects the rear of the floating array with a polyether ether ketone (PEEK) microfluidic adapter of 12 × 12 × 5 mm³, also shown in figure 4(a). This adapter serves as a fluidic interface between the external fluid supply and the microfluidic cable. Therefore, one end of the cable is

Table 2. Material properties of different materials considered for the microfluidic cable. Data are extracted from technical datasheets if not indicated otherwise.

	Processing viscosity (mPas)	Hardness (Shore A)	Young's modulus (MPa)
Parylene-C [58]	–	–	3200
Polyimide [59]	–	–	8500
Silicones:			
Sylgard® 184 [60]	3900	50	1.8 [57]
RTV615 [61]	4000	44	1.5 [57]
MED-6015 (restr.) [62]	~6000	50	~7 ^a
MED-6215 (unrestr.)			
MED-1000 (restr.) [63]	~250 000 ^a	25	~1 ^a
MED-2000 (unrestr.)			

^a Values estimated by manufacturer.

adapted to the dimensions of the adapter, whereas the other end meets the dimensions of the platform of the array. This results in a tapered shape of the cable. However, to increase the mechanical flexibility of the cable, the tapered parts of the cable may be replaced by a slender rectangular section. Corresponding marks used for dicing purposes are included in the layout as well. Openings in the cable enable the access to the fluidic microchannels in the bonding areas of the adapter and array.

The microfluidic cable is fabricated by replica moulding and plasma bonding of two PDMS membranes, as illustrated in figure 9. Typically, heat-curable two-component addition-cured types of PDMS such as Sylgard® 184 (Dow Corning® Corp., Midland, MI, USA) and RTV615 (Momentive Performance Materials Inc., Albany, NY, USA) are used in MEMS replica moulding [57]. These materials combine low hardnesses of 40–50 Shore A with reasonably low viscosities on the order of 4000 mPas, as summarized in table 2. This enables the membranes to be fabricated by spin-coating. However, both PDMS types are not certified for medical use. On the other hand, one-component condensation-cured silicones certified for medical applications such as MED-2000 (NuSil Technology, Carpinteria, CA, USA) with a hardness of 25 Shore A have estimated viscosities on the order of 250 000 mPas (cf table 2) and require additional dilution with solvents, e.g. n-heptane at a volume ratio of 1:1 [46], to be processed by spin-coating. Therefore, we selected an alternative silicone type, i.e. MED-6215 (NuSil Technology, Carpinteria, CA, USA), which overcomes the mentioned drawbacks. MED-6215 is a heat-curable two-component addition-cured unrestricted medical grade silicone with a hardness of 50 Shore A. It can be directly spin-coated without further dilution due to its low viscosity of 6000 mPas. Since the physical properties of the restricted and unrestricted versions of NuSil silicones are identical, we used the restricted version MED-6015 for first processing tests.

The negative master structure to realize the fluidic microchannels is first fabricated by spin-coating and photolithographically patterning of a 50 μm thick layer of SU-8 photoresist (SU-8 50, MicroChem Corp., Newton, MA, USA) on a polished 4" silicon wafer, as shown in figure 9(a). MED-6015 is prepared at a ratio of 10:1 (base:curing-agent),

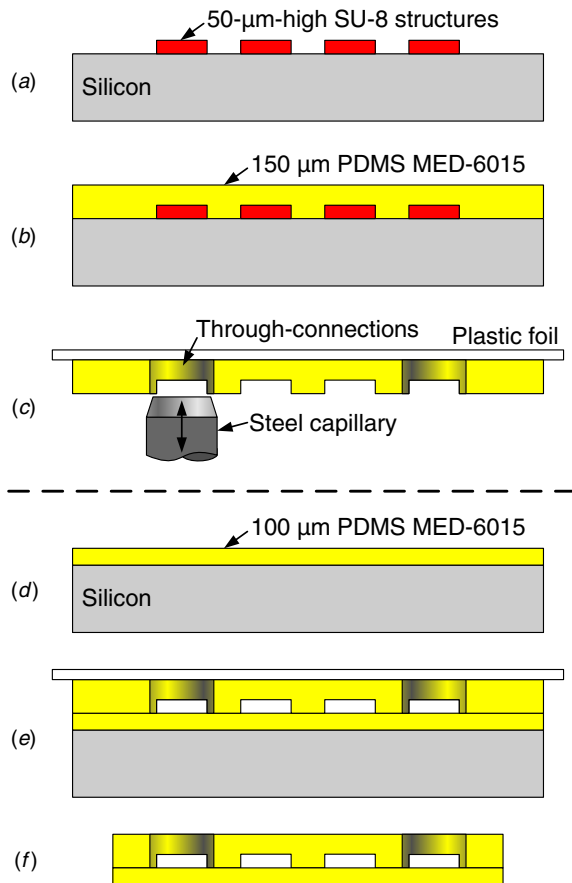


Figure 9. Fabrication process of the microfluidic cable: (a) patterning of SU-8 photoresist on a silicon wafer, (b) replica moulding with PDMS, (c) release of the complete replica and punching-out of through-holes, (d) spin-coating of a PDMS membrane on a bare silicon wafer, (e) full wafer bond of the replica to the membrane, and (f) release of the bonded structure and cutting of the cables.

degassed, spin-coated over the silanized SU-8 structure to a PDMS membrane thickness of $150\ \mu\text{m}$, and heat cured at $80\ ^\circ\text{C}$ for 1 h (cf figure 9(b)). The structured PDMS membrane is then released from the wafer as a whole and adhesively placed on a plastic foil for further handling. Through-connections with a diameter of $600\ \mu\text{m}$ are then punched out at the bonding areas for the fluidic adapter and the platform using a sharpened steel capillary, as illustrated in figure 9(c).

In parallel, an unstructured $100\ \mu\text{m}$ thick PDMS membrane is realized on a polished and silanized $4''$ silicon wafer (cf figure 9(d)). This is followed by the plasma activation of the structured as well as the unstructured membrane in an oxygen plasma (33 W, 2 min) and bonding of the membranes on the wafer level (cf figure 9(e)). The handle foil and bond wafer are removed after 24 h to release the full-wafer bond. Finally, individual cables are separated by cutting the membrane stack along the alignment marks, as shown in figure 9(f).

Figure 10(a) shows an image of the completed microfluidic cable. The SEM micrograph in figure 10(b) depicts a cross-sectional view through a cable section with four microfluidic channels.

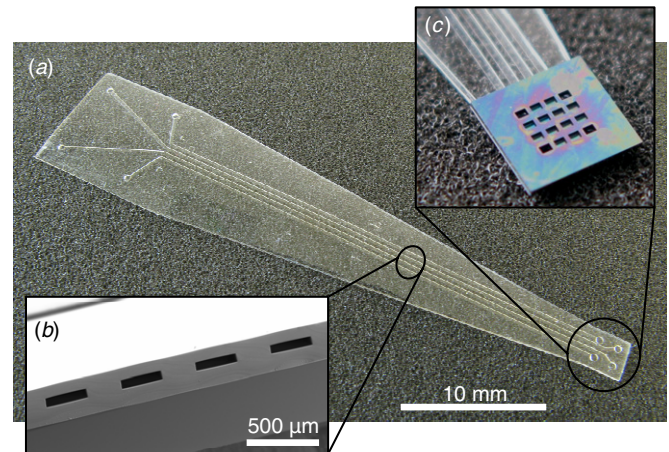


Figure 10. (a) Fabricated microfluidic cable, (b) SEM micrograph of a cross-section of the microfluidic cable with four microchannels and (c) close-up view of a silicon platform attached to the cable.

3.4. Array assembly

The assembly of the floating fluidic array is schematically illustrated in figure 2. In the case of the probe sealing from the bay side and neglecting the steps required for the electrical system functionality, the system assembly starts with bonding the microfluidic cable to the rear side of the platform. For this purpose, the microfluidic cable is adhesively fixed on a plastic foil which serves as a carrier to facilitate the cable handling. The bond between the cable and the rear side of the platform is realized by plasma activation of the microfluidic cable as well as the platform in an oxygen plasma (33 W, 2 min) and bringing both components into contact. Since the round openings of the cable have to precisely match the through-connections of the platform, alignment and bonding is performed on a flip-chip bonder (FINEPLACER[®], Finetech GmbH & Co. KG, Berlin, Germany). A close-up view of a silicon platform assembled to the cable tip is shown in figure 10(c). In the next step, the probe combs are individually inserted into the platform. This is realized using a flip-chip bonder (FC150, SET, Saint Jeoire, France) with a custom-made tooling chuck according to the procedure described elsewhere [50]. Once the combs are inserted, the remaining gaps between the probe base segments and the sidewalls of the bays are filled with epoxy resin manually dispensed from the bay side of the platform. In contrast to the epoxy resin EPO-TEK[®] 353ND used in the case of the test structures, EPO-TEK[®] 301 with a viscosity lower by more than one order of magnitude was used. The low viscosity enables the adhesive to creep within its pot life into the remaining probe-platform gaps by capillary forces resulting in leakage-tight sealing. In this case, the gaps around the fluidic inlet segments on the platform rear serve as capillary stops preventing the adhesive from entering the microfluidic channels of the cable. The epoxy is then cured at room temperature for 24 h. A floating array with two fluidic probe combs of type P1 is shown in figure 11(c) with the cable fixed on the carrier foil. As the two non-fluidic probe combs in the middle of the platform are not required to demonstrate the fluidic functionality, these two combs have not been inserted.

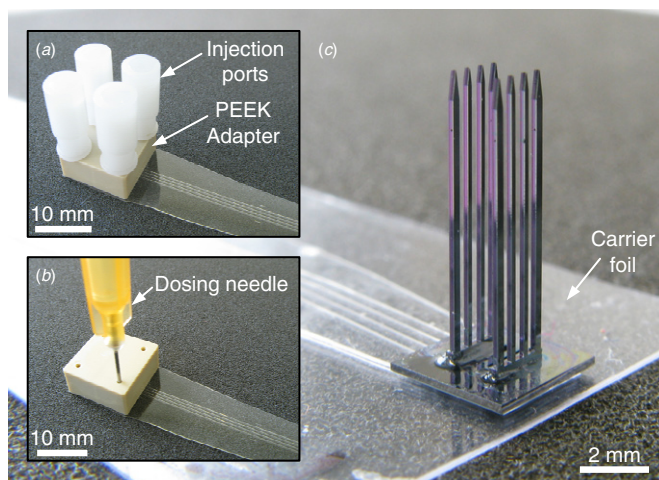


Figure 11. Optical micrographs of the PEEK adapter with (a) injection ports or (b) a dosing needle to access the four channels of the microfluidic cable, and (c) an assembled fluidic array with two four-shaft combs sealed with the adhesive. The system is placed on a carrier foil for handling purposes during testing.

To realize liquid supply to the microfluidic cable and consequently to the whole array, an adapter is required. Preferably, the adapter allows for a flexible connection and disconnection of a variety of external fluidic equipment, e.g. syringe pumps. As shown in figure 11(a), an adapter capable to carry up to four commercially available miniature tubing injection ports (SIP22/4, Instech Laboratories Inc., Plymouth Meeting, PA, USA) was implemented for this purpose. Alternatively, the adapter can be used to connect the microfluidic cable directly with gauge 22 dispensing needles (cf figure 11(b)), e.g. for fluidic characterization purposes.

The adapter with a size of $12 \times 12 \times 5 \text{ mm}^3$ has four through-connections with a diameter of $700 \mu\text{m}$ and is made of PEEK. To realize the bond between the cable and the PEEK adapter, the bottom of the adapter is pre-treated with an adhesion promoter and spin-coated with a thin layer of MED-6015 cured at $80 \text{ }^\circ\text{C}$ for 1 h. After removal of the PDMS in the through-connections

of the adapter, its bottom side as well as the corresponding section of the microfluidic cable is activated in an oxygen plasma with the same parameters as given above. Since the through-connections of the adapter have to precisely match the openings in the fluidic cable, the adapter is aligned with respect to the cable using a flip-chip bonder and the bond partners are brought together. The steel capillaries of the miniature injection ports are finally inserted into the adapter and optionally sealed with an adhesive. As an example, figure 12(a) shows an array comprising two fluidic probes of type P1.

4. Experimental results

The liquid delivery capability of the arrays was demonstrated by using a completely assembled device partially immersed into water. The corresponding experimental setup with the array kept on the carrier foil used during fabrication and additionally secured with an adhesive tape is shown in figure 12(a). The four microfluidic channels were successively provided with a coloured liquid which was manually released using a syringe. Figure 12(b) shows an optical micrograph of a representative liquid released from one of the probe shafts. Although the blockage of the fluidic microchannels due to the applied adhesive of low viscosity was initially considered to be a potential risk, no blocked channels were observed so far. Thus, bay-side sealing turned out to be a viable approach.

Furthermore, the liquid delivery of the array was quantitatively characterized at $22 \text{ }^\circ\text{C}$. In this case, the partially immersed array was connected to an elevated reservoir filled with $0.45 \mu\text{m}$ filtered deionized water. The resulting flow rate as a function of the applied hydrostatic pressure was measured with a commercial flow sensor (μ -FLOW, Bronkhorst Mätting GmbH, Kamen, Germany) positioned in-line between the reservoir and the array. The representative measurements of the four channels of the array are shown in figure 13. As expected from laminar flow theory, a linear relation between the applied pressure and the resulting flow rate is obtained. The small difference of around 8% in the flow rates of channels

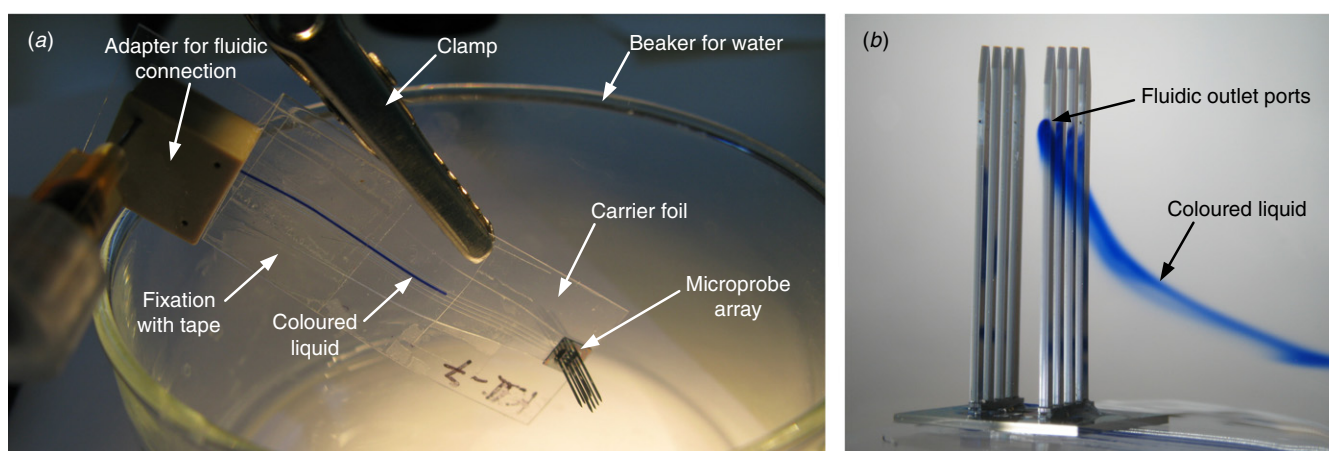


Figure 12. (a) Assembled floating array placed on a carrier foil and fixed with an adhesive tape. The array is fluidically connected to a dosing needle, lowered into a glass beaker with water and filled with a coloured liquid; (b) immersion of the array into clear water and release of coloured liquid from one probe shaft.

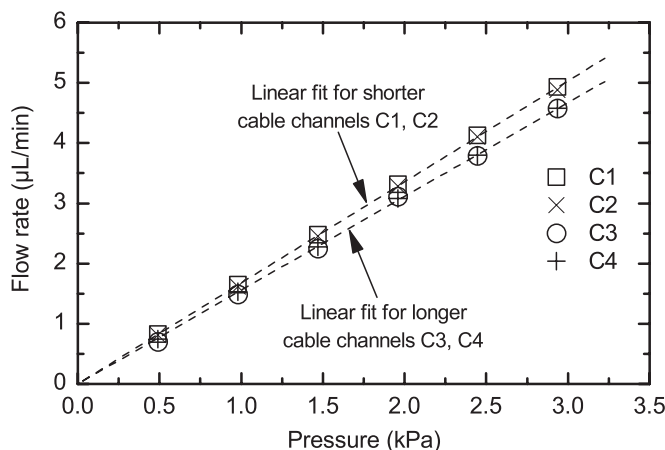


Figure 13. Measured flow rate versus applied hydrostatic pressure for the four channels C1–C4 of an array. The characterization was performed according to the setup shown in figure 12(a) using 0.45 μm filtered deionized water at 22 $^{\circ}\text{C}$.

C1, C2 versus C3, C4 can be explained by the two different channel layouts shown in figure 4(b). For identical types of probe combs, the lower resistance of the shorter channels C1, C2 can be clearly distinguished from the longer channels C3, C4 as indicated in figure 13.

Aside from these purely fluidic characteristics of the neural probes in combination with the microfluidic cable, the diffusive water vapour and liquid water transport through the cable walls, i.e. the vapour and liquid transmission rates, respectively, are of particular importance in view of the system performance. In general, high mechanical elasticity of polymers is always related to weak cross-linking of the molecular chains [64] which promotes the diffusive transport across the material. As an example, the microfluidic cable is filled under operational conditions with the drug liquid and is at the same time surrounded by the cerebrospinal fluid (CSF). Due to the different species concentrations in both liquids, diffusion-driven osmotic transport into and out of the microfluidic cable will take place. Thereby, the thinnest wall thickness of the cable is 100 μm . Furthermore, the evaporation of liquid through the cable has to be considered as well for those cable sections exposed to the atmosphere. In both cases, the transmission through the cable can be reduced using additional barrier materials deposited onto the cable surface. As parylene-C has already been tested as a potential candidate for the encapsulation of the entire platform including its electrical contacts [65], it has been considered as a barrier material for the microfluidic cable as well.

In order to evaluate the effect of parylene-C on the water vapour and liquid transmission rates of the microfluidic cables, 100 μm thin PDMS membranes were realized, as described above. Optionally, this was followed by the chemical vapour deposition of a 2.5 μm thin parylene-C layer (C50F, COMELEC SA, La Chaux-de-Fonds, Switzerland, with dimer diX C, Daisan Kasei Co., Ltd, Tokyo, Japan) on one side of the membrane. Although it is in general very difficult to reproduce the operational conditions in the brain as various ionic and molecular species are present at variable concentrations in the

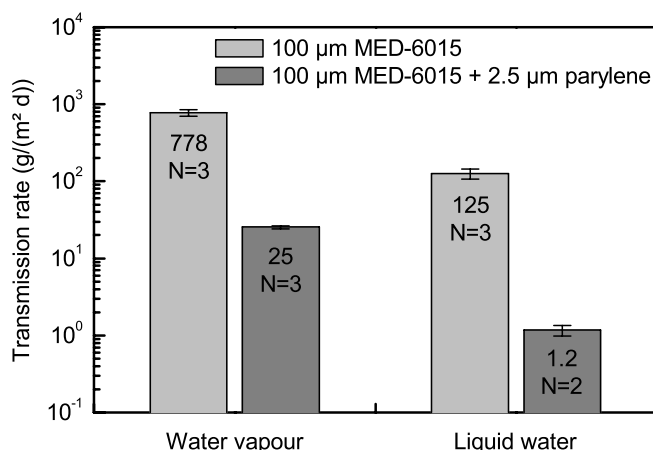


Figure 14. Water vapour and osmotic liquid water transmission rates of MED-6015 membranes with and without one-sided parylene-C coating (water vapour: $T = 39 \pm 2$ $^{\circ}\text{C}$, $\Delta rH = 86 \pm 2\%$; liquid water: $T = 23 \pm 2$ $^{\circ}\text{C}$, $\Delta p_{\text{osmose}} = 36$ MPa; N = number of experiments).

CSF, worst case estimates of the transmission rates can be determined.

In this study, the water vapour transmission rates were determined based on the Water Method [66]. For this purpose, glass cups (diameter 75 mm) were filled with water and sealed with a membrane made of either bare PDMS or PDMS covered by a parylene-C layer. The cups were stored at a temperature of $T = 39 \pm 2$ $^{\circ}\text{C}$. Considering the saturated vapour atmosphere inside the cups, a relative humidity difference of $\Delta rH = 86 \pm 2\%$ across the membranes was maintained. During storage, the weight loss of the cups was monitored over a time frame of 4 days resulting in the averaged water vapour transmission rate. In the case of bare MED-6015, this transmission rate can be translated into a material specific property, i.e. the water vapour permeability. The determined value of 13.6 $\mu\text{g}/(\text{Pa m d})$ is in good agreement with measurements previously performed with a similar type of PDMS [67]. As illustrated in figure 14, the parylene-C coating reduces the vapour transmission rate by a factor of approximately 30. For the 40 mm long cable segment between the fluidic adapter and the silicon platform, this result corresponds to an absolute reduction of the liquid loss through the two cable walls of one channel from 18.8 to 0.6 $\mu\text{L}/\text{day}$. However, in reality, it is expected that the vapour transmission rate will be only of minor relevance since the cable is filled and surrounded by liquids.

In contrast, the liquid water transmission rate of the cables due to osmotic forces is more critical. Therefore, the transmission rates were determined by measuring the osmotic flows across the membranes with a diameter of 82 mm separating deionized water and saturated sodium chloride (NaCl) solution. The membranes were mounted into a commercial stainless steel membrane holder. One side of the membrane holder was supplied with deionized water, whereas the second side was connected to a reservoir filled with a saturated NaCl solution and placed on a microbalance. Following basic osmotic laws for the saturated NaCl solution, this results in an osmotic pressure difference on the order of

$\Delta p_{Osmose} = 36$ MPa across the membranes [68]. The entire setup was held at $T = 23 \pm 2$ °C. The liquid water transmission rate was then extracted from the linear weight increase of the reservoir due to the osmotic flow. The difference between the uncoated and the parylene-coated membranes is illustrated in figure 14. The parylene film reduces the water transmission rate by a factor of 100. Relating this result to the two thin walls of one channel in the 40 mm long cable segment between the fluidic adapter and the silicon platform, this corresponds to an absolute reduction of the liquid flow into the cable from 3 to 0.03 $\mu\text{L}/\text{day}$. Since increasing temperature promotes diffusive processes, the transmission is expected to increase further with body temperature.

In both cases, the parylene-C coating significantly reduces water vapour and liquid water transmission. Unfortunately, the Young's modulus of parylene-C is larger by a factor of around 450 compared to that of MED-6015 (cf table 2). Consequently, the parylene-C coating with a thickness of 2.5 μm noticeably stiffens the cable.

5. Discussion and conclusion

This paper presented the first 3D floating silicon array for drug delivery in neuroscience. The array comprises a silicon platform into which individual probe combs can be inserted as well as a microfluidic cable with an adapter used for liquid supply. Due to the full compatibility of the fluidic integration concept with the assembly of an array with recording electrodes reported previously [27, 37], this is the first step towards a multifunctional floating array which combines drug delivery and electrical recording.

The fabrication process of the probe combs is based on a two-stage DRIE process combined with silicon wafer bonding and grinding that offers great flexibility in the design of the probe shape as well as the fluidic microchannels [20]. This enables in-plane fluidic inlet ports to be realized in the segments of the probe comb used for probe fixation in the platform. Although the fluidic inlet segments have to be located at specific positions in the platform, the comb base can be used to distribute the two fluidic microchannels to virtually any position on the probe comb. Consequently, selected shafts might be equipped with either one or two independent fluidic channels. This offers great flexibility in designing application-specific probe combs as demonstrated by the two comb designs P1 and P2. In the case of design P1, liquids can be infused independently from two different shafts maximizing the volume coverage in the brain. On the other hand, design P2 has a central fluidic shaft incorporating two independent microchannels with outlets just separated by the shaft width of 250 μm . Consequently, two different liquids, e.g. a drug and a buffer reference, can be infused at almost the same location.

The integration concept foresees the implementation of the fluidic cable on the rear of the platform, while an electric cable will be mounted on its front side. This geometry maximizes the space available on the floating platform. On the other hand, the bay side is solely dedicated to the electrodes connection, and the rear side is reserved for the liquid supply.

Moreover, the sealing process of the fluidic probe combs developed in this study requires no additional process steps compared to the assembly of an electric array without liquid delivery [27].

Neglecting the height of the comb bases, the realized array including the microfluidic cable has a total backbone thickness of only 550 μm comparable to slim-backbone silicon arrays restricted to electrical recording [25–28].

Liquid supply to the array as well as its floating operation is enabled by the highly elastic microfluidic cable. In contrast to the typically used silicones in MEMS technology, the selected medical grade silicone type MED-6015/MED-6025 (restricted/unrestricted) enables the compliance with the regulations for implantable devices. Additionally, the silicone type selected in this work can be spin-coated directly without the need for a further viscosity reduction by dilution with potentially hazardous solvents as it is the case for one-component condensation-cured silicones.

However, whereas the high flexibility of the microfluidic cable is desirable with respect to the floating operation of the array, this results in several drawbacks. Typically, elastic microfluidic structures are omitted if not explicitly required. The reason for this is related to the fact that elastic channel walls allow the fluidic channels to expand upon pressurizing the liquid. Consequently, the whole channel structure serves as a fluidic capacitor which can store and release liquid depending on the actual pressure condition. This can alter the transient infusion profile. Based on preliminary finite element simulations, a volume increase of the fluidic microchannels of around 5% is estimated assuming a liquid pressure of 10 kPa accounting for dynamic pressure variations as well as the unpredictable backpressure from the brain. Moreover, mechanical movements of the cable can deform the fluidic microchannels, thereby causing unintentional liquid infusion or suction. Additionally, increasing liquid pressures in the cable and the associated mechanical deformation can stiffen the cable.

Since the diffusive transport of water vapour and liquid water through the walls of the microfluidic cable are also of concern, the corresponding transmission rates were experimentally determined. However, the applied experimental conditions correspond to worst case scenarios which will normally not be met in reality. Hence, the extracted transmission rates allow only the estimation of the maximum diffusive flows and the order of magnitude by which parylene-C coating can reduce them. The vapour and liquid transmission rates through the cable walls were reduced by a 2.5 μm thin parylene-C coating from 18.6 to 0.6 $\mu\text{L}/\text{day}$ and 3 to 0.03 $\mu\text{L}/\text{day}$, respectively. Any flow into the cable will consequently displace the drug liquid and cause unintended delivery. In turn, flows out of cable result in suction of CSF into the microprobes. From the application point of view, water transmission due to osmosis is considered to be most relevant. Considering the drug volume of 0.9 μL stored in cable and probes, this volume would be completely displaced (i.e. infused) by osmotic flows through the cable walls within 7 h. In contrast, according to this worst case scenario, cables coated by parylene-C will exhibit this effect over a time frame of 1 month.

However, to evaluate the actual transmission rates as well as the necessity of an additional barrier, experiments closer to *in vivo* conditions applying the respective liquids have to be performed. In general, the additional parylene-C coating should only be applied if it is inevitable since it increases the cable stiffness and further complicates the fabrication process.

In view of smallest liquid volumes to be dispensed, the dead volume of the entire fluidic system has to be taken into account. In the case of the actual probe design, 9 μL of liquid is stored in total in one channel of the microprobe, microfluidic cable and injection port. Thereby, 8 μL is contributed by the injection port. Hence, for infusions smaller than 9 μL , only liquid already stored in the array is actually infused. Although injection ports are currently the components of choice with respect to pluggable and self-sealing fluidic micro connections, they contribute 90% of the dead volume of the described liquid system. In addition, a liquid displacement of at least 1 μL has to be taken into account during insertion and backtrack of the septum needle in the injection port causing infusion and suction, respectively. Therefore, the septum connection is certainly one main point to be addressed in the future. Since no pluggable fluidic micro connectors with the required specifications are currently available, one possible solution is the direct connection with a miniaturized drug delivery mechanism such as the recently presented *NeuroMedicator* [69] which can remain next to the array.

Future work has to concentrate first and foremost on the integration of the recording electrodes. The full compatibility with the electric integration concept presented previously [27, 50] is already ensured. All shafts of the presented probe combs are prepared to carry additional electrodes. This opens the perspective to simultaneously infuse drugs and monitor neural activity. While the electrodes on the fluidic probe shafts could be affected by a potential liquid backflow [55], the electrodes on the separate non-fluidic shaft will not be affected by this phenomenon.

Previously, 2D probe combs for drug delivery and electrode recording based on the same core fabrication technology as used in this study have been successfully tested *in vivo* [35]. For the future, integration of additional functionalities beyond electric recording will be addressed. This includes biosensors on the probe shafts which can be directly calibrated *in vivo* by using liquids provided by the fluidic microchannels in the array. For this reason, silicon microprobes with integrated microfluidic channels and glutamate biosensors have already been fabricated [70] based on the core technologies demonstrated within *NeuroProbes* [48].

Acknowledgments

This work was performed in the frame of the Information Society Technologies (IST) Integrated Project *NeuroProbes* of the 6th Framework Program (FP6) of the European Commission (Project number IST-027017). The authors gratefully acknowledge the support from the cleanroom facilities at HSG-IMIT, IMTEK and IMEC for wafer processing and process optimization. Furthermore, the authors

would like to thank Roland Gronmaier and Garance Degret (both HSG-IMIT) for preliminary studies on the microfluidic cable and Herbert Straatman (HSG-IMIT) for taking the SEM micrographs.

References

- [1] Kandel E R 2000 Nerve cells and behavior *Principles of Neural Science* ed E R Kandel *et al* (New York: McGraw-Hill)
- [2] Lehw G and Nicolelis M A L 2008 State-of-the-art microwire array design for chronic neural recordings in behaving animals *Methods for Neural Ensemble Recordings* ed M A L Nicolelis (Boca Raton: CRC Press)
- [3] Malpeli J G 1999 Reversible inactivation of subcortical sites by drug injection *J. Neurosci. Methods* **86** 119–28
- [4] Hajj Hassan M, Chodavarapu V and Musallam S 2008 NeuroMEMS: neural probe microtechnologies *Sensors* **8** 6704–26
- [5] Floating Microelectrode Arrays (Gaithersburg, USA: MicroProbes for Life Science) www.microprobes.com (accessed 12/06/2011)
- [6] Plexon Plextrode[®] Floating Microelectrode Array (Dallas, USA: Plexon Inc.) www.plexon.com (accessed 12/06/2011)
- [7] Musallam S, Bak M J, Troyk P R and Andersen R A 2007 A floating metal microelectrode array for chronic implantation *J. Neurosci. Methods* **160** 122–27
- [8] Bradley D C *et al* 2005 Visuotopic mapping through a multichannel stimulating implant in primate V1 *J. Neurophysiol.* **93** 1659–70
- [9] Campbell P K, Jones K E, Huber R J, Horch K W and Normann R A 1991 A silicon-based, three-dimensional neural interface: manufacturing processes for an intracortical electrode array *IEEE Trans. Biomed. Eng.* **38** 758–68
- [10] Harrison R R, Kier R J, Chestek C A, Gilja V, Nuyujukian P, Ryu S, Greger B, Solzbacher F and Shenoy K V 2009 Wireless neural recording with signal low-power integrated circuit *IEEE Trans. Neural Syst. Rehabil. Eng.* **17** 322–29
- [11] Reed M L and Lye W-K 2004 Microsystems for drug and gene delivery *Proc. IEEE* **92** 56–75
- [12] Hoogerwerf A C and Wise K D 1994 A three-dimensional microelectrode array for chronic neural recording *IEEE Trans. Biomed. Eng.* **41** 1136–46
- [13] Norlin P, Kindlundh M, Mouroux A, Yoshida K and Hofmann U G 2002 A 32-site neural recording probe fabricated by DRIE of SOI substrates *J. Micromech. Microeng.* **12** 414–9
- [14] Ruther P, Herwik S, Kisban S, Seidl K and Paul O 2010 Recent progress in neural probes using silicon MEMS technology *IEEE Trans. Electr. Electron. Eng.* **5** 505–15
- [15] Motta P S and Judy J W 2005 Multielectrode microprobes for deep-brain stimulation fabricated with a customizable 3D electroplating process *IEEE Trans. Biomed. Eng.* **52** 923–33
- [16] Musa S, Welkenhuysen M, Huys R, Eberle W, van Kuyck K, Bartic C, Nuttin B and Borghs G 2009 Planar 2D-array neural probe for deep brain stimulation and recording (DBSR) *Proc. 4th Eur. Conf. of the IFMBE (Antwerp, Belgium, 2008)* vol 22 ed J Vander Sloten *et al* (Berlin: Springer) pp 2421–25
- [17] Najafi K, Wise K D and Mochizuki T 1985 A high-yield IC-compatible multichannel recording array *IEEE Trans. Electron Devices* **32** 1206–11
- [18] Seidl K, Herwik S, Torfs T, Neves H, Paul O and Ruther P 2011 CMOS-based high-density silicon microprobe array for electronic depth control in intracortical neural recording *J. Microelectromech. Syst.* [at press](#)

- [19] Chen J, Wise K D, Hetke J F and Bledsoe S C Jr 1997 A multichannel neural probe for selective chemical delivery at the cellular level *IEEE Trans. Biomed. Eng.* **44** 760–9
- [20] Seidl K, Spieth S, Herwik S, Steigert J, Zengerle R, Paul O and Ruther P 2010 In-plane silicon probes for simultaneous neural recording and drug delivery *J. Micromech. Microeng.* **20** 105006
- [21] Johnson M D, Franklin R K, Gibson M D, Brown R B and Kipke D R 2008 Implantable microelectrode arrays for simultaneous electrophysiological and neurochemical recordings *J. Neurosci. Methods* **174** 62–70
- [22] Frey O, Holtzman T, McNamara R M, Theobald D E H, van der Wal P D, de Rooij N F, Dalley J W and Koudelka-Hep M 2010 Enzyme-based choline and l-glutamate biosensor electrodes on silicon microprobe arrays *Biosens. Bioelectron.* **26** 477–84
- [23] Wise K D, Angell J B and Starr A 1970 An integrated-circuit approach to extracellular microelectrodes *IEEE Trans. Biomed. Eng.* **17** 238–47
- [24] Yao Y, Gulari M N, Wiler J A and Wise K D 2007 A microassembled low-profile three-dimensional microelectrode array for neural prosthesis applications *J. Microelectromech. Syst.* **16** 977–88
- [25] Perlin G E and Wise K D 2010 An ultra compact integrated front end for wireless neural recording microsystems *J. Microelectromech. Syst.* **19** 1409–21
- [26] Merriam M E, Dehmel S, Srivannavit O, Shore S E and Wise K D 2011 A 3D 160-site microelectrode array for cochlear nucleus mapping *IEEE Trans. Biomed. Eng.* **58** 397–403
- [27] Aarts A A A et al 2008 A 3D slim-base probe array for *in vivo* recorded neuron activity *Proc. 30th Annu. Int. Conf. of the IEEE EMBS (Vancouver, BC, Canada, 2008)* pp 5798–801
- [28] Kisban S, Holzhammer T, Herwik S, Paul O and Ruther P 2010 Novel method for the assembly and electrical contacting of out-of-plane microstructures *Proc. 23rd IEEE Int. Conf. on MEMS (Hong Kong, 2010)* pp 484–7
- [29] Lee Y-T, Lin C-W, Lin C-M, Yeh S-R, Chang Y-C and Fang W 2010 A pseudo 3D glass microprobe array: glass microprobe with embedded silicon for alignment and electrical interconnection during assembly *J. Micromech. Microeng.* **20** 025014
- [30] Pang C, Musallam S, Tai Y-C, Burdick J W and Andersen R A 2006 Novel monolithic silicon probes with flexible parylene cables for neural prostheses *Proc. Int. Conf. on Microtechn. in Med. and Biol. (Okinawa, Japan, 2006)* pp 64–7
- [31] NeuroNexus 3D probe assembly and package (Ann Arbor, USA: NeuroNexus Technologies, Inc.) www.neuronexustech.com (accessed 12/06/2011)
- [32] Du J, Roukes M L and Masmanidis S C 2009 Dual-side and three-dimensional microelectrode arrays fabricated from ultra-thin silicon substrates *J. Micromech. Microeng.* **19** 075008
- [33] Takeuchi S, Suzuki T, Mabuchi K and Fujita H 2004 3D flexible multichannel neural probe array *J. Micromech. Microeng.* **14** 104–7
- [34] Wang M-F, Maleki T and Ziaie B 2010 A self-assembled 3D microelectrode array *J. Micromech. Microeng.* **20** 035013
- [35] Spieth S, Schumacher A, Seidl K, Hiltmann K, Haeberle S, McNamara R, Dalley J W, Edgley S A, Ruther P and Zengerle R 2009 Robust microprobe systems for simultaneous neural recording and drug delivery *Proc. 4th Eur. Conf. of the IFMBE (Antwerp, Belgium, 2008)* vol 22 ed J Vander Sloten et al (Berlin: Springer) pp 2426–30
- [36] Hetke J F, Williams J C, Pellinen D S, Vetter R J and Kipke D R 2003 3D silicon probe array with hybrid polymer interconnect for chronic cortical recording *Proc. 1st Int. IEEE EMBS Conf. on Neural Eng. (Capri Island, Italy, 2003)* pp 181–4
- [37] Herwik S, Kisban S, Aarts A A A, Seidl K, Girardeau G, Benchenane K, Zugaro M B, Wiener S I, Paul O and Ruther P 2009 Fabrication technology for silicon-based microprobe arrays used in acute and sub-chronic neural recording *J. Micromech. Microeng.* **19** 074008
- [38] Perlin G E and Wise K D 2009 Ultra-compact integration for fully-implantable neural microsystems *Proc. 22nd IEEE Int. Conf. on MEMS (Sorrento, Italy, 2009)* pp 228–31
- [39] Metz S, Bertsch A, Bertrand D and Renaud P 2004 Flexible polyimide probes with microelectrodes and embedded microfluidic channels for simultaneous drug delivery and multi-channel monitoring of bioelectric activity *Biosens. Bioelectron.* **19** 1309–18
- [40] Takeuchi S, Ziegler D, Yoshida Y, Mabuchi K and Suzuki T 2005 Parylene flexible neural probes integrated with microfluidic channels *Lab Chip* **5** 519–23
- [41] Ziegler D, Suzuki T and Takeuchi S 2006 Fabrication of flexible neural probes with built-in microfluidic channels by thermal bonding of parylene *J. Microelectromech. Syst.* **15** 1477–82
- [42] Duffy D C, McDonald J C, Schueller O J A and Whitesides G M 1998 Rapid prototyping of microfluidic systems in poly(dimethylsiloxane) *Anal. Chem.* **70** 4974–84
- [43] Xia Y and Whitesides G M 1998 Soft lithography *Annu. Rev. Mater. Sci.* **28** 153–84
- [44] Curtis J and Colas A 2004 Medical applications of silicones *Biomaterials Science* ed B D Ratner et al (Amsterdam: Elsevier)
- [45] Maghribi M, Hamilton J, Polla D, Rose K, Wilson T and Krulevitch P 2002 Stretchable micro-electrode array *Proc. 2nd Ann. Int. IEEE-EMBS Special Topic Conf. on Microtechn. in Med. and Biol. (Madison, WI, USA, 2002)* pp 80–3
- [46] Schuettler M, Stiess S, King B V and Suaning G J 2005 Fabrication of implantable microelectrode arrays by laser cutting of silicone rubber and platinum foil *J. Neural Eng.* **2** S121–28
- [47] Subbaroyan J and Kipke D R 2006 The role of flexible polymer interconnects in chronic tissue response induced by intracortical microelectrodes—a modeling and an *in vivo* study *Proc. 28th Annu. Int. Conf. of the IEEE EMBS (New York City, NY, USA, 2006)* pp 3588–91
- [48] Neves H P, Orban G A, Koudelka-Hep M and Ruther P 2007 Development of multifunctional probe arrays for cerebral applications *Proc. 3rd Int. IEEE EMBS Conf. on Neural Eng. (Kohala Coast, HI, USA, 2007)* pp 104–9
- [49] Ruther P et al 2008 The NeuroProbes project—multifunctional probe arrays for neural recording and stimulation *Biomed. Tech.* **53** 238–40
- [50] Aarts A A A, Neves H P, Puers R P and Van Hoof C 2008 An interconnect for out-of-plane assembled biomedical probe arrays *J. Micromech. Microeng.* **18** 064004
- [51] Aarts A A A, Neves H P, Puers R P, Herwik S, Seidl K and Ruther P 2009 A slim out-of-plane 3D implantable CMOS based probe array *Proc. Smart Systems Integration (Brussels, Belgium, 2009)* pp 258–63
- [52] Kisban S, Janssen P, Herwik S, Stieglitz T, Paul O and Ruther P 2008 Hybrid microprobes for chronic implantation in the cerebral cortex *Proc. 30th Annu. Int. Conf. of the IEEE EMBS (Vancouver, BC, Canada, 2008)* pp 2016–19
- [53] Meyer J-U, Stieglitz T, Scholz O, Haberer W and Beutel H 2001 High density interconnects and flexible hybrid assemblies for active biomedical implants *IEEE Trans. Adv. Packag.* **24** 366–74

- [54] Kisban S, Kennntner J, Janssen P, von Metzen R, Herwik S, Bartsch U, Stieglitz T, Paul O and Ruther P 2009 A novel assembly method for silicon-based neural devices *Proc. World Cong. on Med. Physics and Biomed. Eng. (Munich, Germany, 2009) (IFMBE Proc. vol 25/9)* ed O Dössel and W C Schlegel (Berlin: Springer) pp 107–10
- [55] Spieth S, Schumacher A, van de Moosdijk S, Haerberle S and Zengerle R 2009 Silicon microprobe systems for neural drug delivery: experimental characterization of liquid distribution *Proc. World Cong. on Med. Physics and Biomed. Eng. (Munich, Germany, 2009) (IFMBE Proc. vol 25/9)* ed O Dössel and W C Schlegel (Berlin: Springer) pp 158–61
- [56] Herwik S, Paul O and Ruther P 2011 Ultrathin silicon chips of arbitrary shape by etching before grinding *J. Microelectromech. Syst.* **20** 791–3
- [57] Schneider F, Fellner T, Wilde J and Wallrabe U 2008 Mechanical properties of silicones for MEMS *J. Micromech. Microeng.* **18** 065008
- [58] Kisco diX C (Tokyo, Japan: Daisan Kasei Co., Ltd) www.kisco-net.co.jp (accessed 12/06/2011)
- [59] HD Microsystems PI-2611 (Parlin, NJ, USA: HD Microsystems) www.hdmicrosystems.com (accessed 12/06/2011)
- [60] Dow Corning Sylgard® 184 silicone encapsulant (Midland, MI, USA: Dow Corning® Corp.) www.dowcorning.com (accessed 12/06/2011)
- [61] Momentive RTV615 silicone rubber compound (Albany, NY, USA: Momentive Performance Materials Inc.) www.momentive.com (accessed 12/06/2011)
- [62] NuSil MED-6015 optically clear potting and encapsulating silicone elastomer (Carpinteria, CA, USA: NuSil Technology) www.nusil.com (accessed 12/06/2011)
- [63] NuSil MED-1000 silicone adhesive (Carpinteria, CA, USA: NuSil Technology) www.nusil.com (accessed 12/06/2011)
- [64] Dominghaus H, Elsner P, Eyerer P and Hirth T 2008 *Kunststoffe: Eigenschaften und Anwendungen* (Berlin: Springer)
- [65] von Metzen R P, Lass N, Ruther P and Stieglitz T 2011 Diffusion-limited deposition of parylene C *J. Microelectromech. Syst.* **20** 239–50
- [66] ASTM 2010 ASTM standard E96/E96M-10 standard test methods for water vapor transmission of materials (West Conshohocken, PA: ASTM International)
- [67] Blume I, Schwering P J F, Mulder M H V and Smolders C A 1991 Vapour sorption and permeation properties of poly(dimethylsiloxane) films *J. Membr. Sci.* **61** 85–97
- [68] Theeuwes F and Ayer A D 1978 Osmotic devices having composite walls *U.S. Patent* 4077407
- [69] Spieth S, Schumacher A, Kallenbach C, Messner S and Zengerle R 2010 NeuroMedicator—a disposable drug delivery system with silicon microprobes for neural research *Proc. 23rd IEEE Int. Conf. on MEMS (Hong Kong, 2010)* pp 983–6
- [70] Frey O, van der Wal P D, Spieth S, Brett O, Seidl K, Paul O, Ruther P, Zengerle R and de Rooij N F 2011 Biosensor microprobes with integrated microfluidic channels for bi-directional neurochemical interaction *J. Neural Eng.* **8** 066001